

Abstract

Given appropriate data acquisition, processing to remove nonprimary arrivals, and use of an accurate migration algorithm, it is the quality of the subsurface velocity model that typically controls the quality of imaging that can be obtained from salt-affected seismic data. Full-waveform inversion has the potential to improve the accuracy, resolution, repeatability, and speed with which such velocity models can be generated, but, in the absence of an accurate starting model, that potential is difficult to realize in practice. Presented are successful inversion results, obtained from synthetic subsalt models, using a robust full-waveform inversion code that includes constraints upon the set of allowable earth models. These constraints include limitations on the total variation of the velocity of the model and, most significantly, on the asymmetric variation of velocity with depth such that negative velocity excursions are limited. During the iteration, these constraints are relaxed progressively so that the final model is driven principally by the seismic data, but the constraints act to steer the inversion path away from local minima in its early stages. This methodology is applied to portions of the 2004 BP benchmark and Phase I SEAM salt models, recovering an accurate model of the salt body, including its base and flanks, and an accurate model of the subsalt velocity structure, starting from one-dimensional velocity models that are severely cycle skipped. This approach removes entirely the requirement to pick salt boundaries from migrated seismic data, and acts as a form of automatic salt and sediment flooding during full-waveform inversion.

Introduction

High-quality imaging of subsalt and salt-affected seismic data in areas that contain geometrically complex salt bodies is seldom easy. Success typically requires appropriate multiazimuth, long-offset, broadband acquisition to provide adequate illumination of the salt-affected target, high-quality noise suppression to remove all but the primary P-wave reflections, sophisticated migration that is able to honor the true subsurface anisotropic velocity model, and a means of building a high-resolution approximation to that velocity model. Although problems can occur in all four of these areas, it is the difficulty of building a sufficiently accurate and well-resolved P-wave velocity model that most often ultimately constrains subsalt image quality; this paper is concerned with addressing that problem.

Typical workflows for subsalt imaging involve the use of reflection traveltime tomography, sometimes supplemented by full-waveform inversion (FWI), to build the shallow postsalt velocity model. This model is first used to depth-migrate and stack limited-offset primary reflection data. The position of top salt is then picked in depth; such picking often involves significant interpretative guidance and human decision making. Once top salt has been

located with confidence, the section is flooded at salt velocity below this picked interface, and the data are remigrated and stacked. The position of bottom salt then can be picked on the remigrated data, and the subsalt section reflooded with sedimentary velocities derived from wells, from a regional compaction trend, or, when circumstances are favorable, from traveltime tomography.

In complicated data sets, this workflow typically involves multiple iterations, multiple passes of tomography, and much testing of different scenarios in which the quality of the final image often is used as the ultimate guide as to the accuracy of the velocity model. While this workflow-based approach often can be successful, it is expensive and time-consuming, it is heavily reliant on the skills and experience of its human practitioners, and there is no guarantee of an ultimately successful outcome. FWI potentially provides a means of building high-resolution high-fidelity velocity models that do not require picking and salt flooding. However, in the absence of an accurate starting model, conventional FWI implementations struggle to build accurate representations of rugose top salt, of the interior of potentially heterogeneous salt bodies, and of complicated salt flanks and base of salt. The role of FWI, therefore, has been limited mostly to only a peripheral one in existing practice.

In this paper we explore an alternative approach in which the velocity model is built predominantly using FWI applied using both refractions and reflections, and in which traveltime tomography, direct picking of salt boundaries, scenario testing, manual salt and sediment flooding, and conventional workflows have no central role to play.

To achieve this, we combine a robust FWI code with a regularization scheme that has been designed specifically to deal effectively with complicated salt bodies. We demonstrate the capabilities of this approach by applying it to synthetic data generated from portions of both the 2004 BP velocity benchmark data set (Billette and Brandsberg-Dahl, 2005) and the Phase I SEAM model (Fehler and Keliher, 2011), and we begin the inversion from a simple one-dimensional starting model that does not contain salt.

Wave-equation-based inversion with constraints

During FWI, we seek to minimize the following data-misfit objective function:

$$f(\mathbf{m}) = \|\mathbf{d}_{\text{obs}} - \mathbf{d}_{\text{sym}}(\mathbf{m})\|^2, \quad (1)$$

where \mathbf{d}_{obs} are the observed data, and $\mathbf{d}_{\text{sym}}(\mathbf{m})$ are simulated data generated by a wave equation which depends on the unknown model parameters \mathbf{m} . While the above problem is easily stated, developing automatic iterative solution techniques that minimize this objective function and produce geologically reasonable velocity

¹Sub Salt Solutions Limited, London.

²The University of British Columbia, Vancouver.

³Imperial College London.

models has proven to be extremely challenging, especially in complex geologic areas including salt plays that are plagued by high-contrast and high-velocity unconformities.

To meet this challenge, industry has so far resorted to labor-intensive workflows that involve picking of reflection events, traveltimes tomography, and salt flooding. While these intricate workflows have proven to be capable of constructing detailed velocity models that produce coherent subsalt images, the results typically are not readily reproducible independently of the expertise and experience of the people involved. Unfortunately, efforts to come up with more automatic and transparent workflows that produce reliable results have been met with mixed success, mainly because these algorithms tend to converge to erroneous local minima.

By combining simple constraints, which encode important generic characteristics of the geology, with multiple cycles of warm-started FWI during which these constraints are relaxed, we arrive at a formulation that is able to recover an accurate velocity field from complex salt-affected geologic models. These constraints remove large areas of the potential solution space that contain local minima by forcing the models to have some predefined characteristics. In practice, if the constraints are well chosen, this approach will slice local minima out of the allowed solution space, and therefore a local iteration scheme will be able to converge toward the true global minimum without requiring that it begins from an unfeasibly accurate starting point.

For velocity models to be geologically plausible, they need to have certain characteristics. These characteristics can be encoded quantitatively as constraints guaranteeing that inverted velocity models comply with our imposed conditions at each stage of the inversion. Mathematically, we guarantee this by ensuring that updated velocity models, i.e. $\mathbf{m}_0 + \Delta\mathbf{m}$ where $\Delta\mathbf{m}$ is the model update with respect to the current model \mathbf{m}_0 , remain in a certain predefined set of feasible models \mathcal{M} . After inclusion of these constraints, FWI aims to find the model \mathbf{m} which minimizes

$$f(\mathbf{m}) \text{ subject to } \mathbf{m}_0 + \Delta\mathbf{m} \in \mathcal{M}. \quad (2)$$

The inversion then proceeds to update the model parameters iteratively in such a way that each new model is projected onto the closest point in the defined constrained set of feasible models \mathcal{M} . When the set is convex, this projection is unique; intersections of convex sets are also convex.

A simple example of a convex set is that generated by applying box constraints, which ensure that the velocity at each grid point

of the inverted velocity model remains within a defined interval that may vary for each grid point. Another example is that obtained by applying structure-promoting constraints, which are typically expressed in terms of some norm. For instance, the set $\mathcal{M}_{\text{TV}} = \{\mathbf{m} : \|\mathbf{m}\|_{\text{TV}} \leq \tau\}$, with τ the size of the total-variation ball, ensures that velocity models are constrained in the total-variation norm defined by

$$\|\mathbf{m}\|_{\text{TV}} = \frac{1}{h} \sum_{ij} \sqrt{(m_{i+1,j} - m_{i,j})^2 + (m_{i,j+1} - m_{i,j})^2}, \quad (3)$$

where h is the grid spacing. Because natural images are often piece-wise smooth, these total-variation norms often are used in image processing to remove noise or to deblur (Rudin et al., 1992).

To illustrate this concept, we can observe how imposing this norm reduces the complexity of the well-known Marmousi velocity model as shown in Figure 1. For small τ , enforcing the box and total-variation norm constraints leads to simplified velocity models with feasible velocities (between $v_{\text{min}} = 1500$ m/s and $v_{\text{max}} = 5500$ m/s in this case) that retain sharp reflectors, as can be seen on the vertical profiles in Figure 1c. If we relax these constraints ($\tau \rightarrow \infty$), then the size of the TV ball increases such that the original model will eventually lie within the constraints \mathcal{M} , at which point the original model will be recovered.

Automatic salt flooding

Salt plays are extremely challenging because they are geologically complex, comprising sedimentary basins interspersed with sharp high-contrast and high-velocity salt bodies. To preserve the distinct nature of salt bodies, researchers (Guo and de Hoop, 2013; Esser et al., 2015) proposed to constrain FWI with the total-variation norm. By construction, this norm is designed to accentuate the interface between the sedimentary embedding and the top, bottom, and flanks of salt. Unfortunately, this approach met with relatively little success because FWI continues to fail for poor starting models and for data that lack ultralow frequencies and ultralong offsets. Through a combination of a new asymmetric hinge-loss constraint and multiple FWI cycles, we overcome this problem.

It is well known that applying FWI without extensive human intervention or without an already accurate starting model has been largely unsuccessful in salt-affected areas. As a result, industry relies on manual workflows that include picking of top and bottom salt, and salt and sediment flooding. As we demonstrate here, the same effect can be produced via a one-sided total-variation constraint, acting in the direction in which the salt continues. For

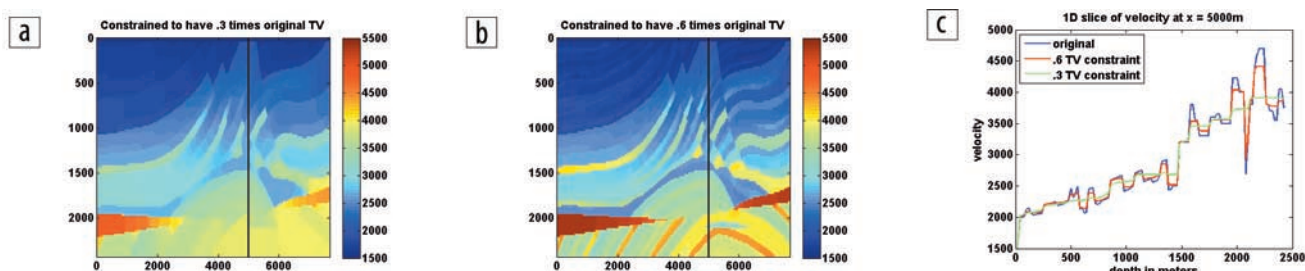


Figure 1. Example of projection onto the intersection of the box constraint for $v_{\text{min}} = 1500$ m/s and $v_{\text{max}} = 5500$ m/s, and a total-variation constraint of (a) $0.3\times$, and (b) $0.6\times$, the original total-variation norm of the Marmousi model. (c) Vertical profile at $x = 5000$ km for the two constrained and the original model. Adapted from Esser et al. (2015).

salt plays that are illuminated from above, this additional asymmetric constraint becomes

$$\|\min(0, D_z \mathbf{m})\|_1 \leq \xi \quad (4)$$

and is given by the sum (the one norm) of the negative vertical finite differences, D_z in velocities. It can be seen as a measure of the velocity decreases in depth. By setting ξ small, we allow inverted velocity models to step into the salt, but we make it unlikely to step out of the salt because we only allow a minor amount of decrease as we step deeper in the model; the trigger for that behavior is that FWI is able to identify top salt as a high-velocity contrast that is then forced to extend in depth. On the other hand, relaxing the constraint by increasing ξ allows velocity models to step down and subsalt velocity lows to build up. This behavior suggests a scheme where we gradually relax the constraint.

In optimization, continuation strategies often are employed to expedite convergence and avoid local minima. Good examples of such a strategy are FWI workflows that start at low frequencies and work their way up to higher frequencies to avoid local minima. Unfortunately, this strategy is inadequate for salt even if we restart FWI beginning with the output of the previous FWI cycle — a technique known to emerge from local minima.

However, if we combine this warm-started FWI technique with a gradual relaxation of the constraints after each cycle, then the inversion results improve dramatically, as shown in Figures 2 through 6. These figures visually demonstrate that this strategy leads to a controlled building of the velocity model as the hinge-loss constraints are gradually relaxed.

Results

The first model we present is the central part of the BP 2004 velocity model (Billette and Brandsberg-Dahl, 2005). FWI without TV or asymmetric TV constraints clearly fails to converge to a global minimum — compare Figures 2b and 2c — because the starting model shown in Figure 2a does not contain accurate low wavenumbers, which causes convergence to a local minimum. When TV and asymmetric TV constraints constrain the inversion, the inversion scheme converges to the much-improved solution shown in Figure 2d.

The salt body in Figure 3 is remarkably well recovered with the proposed method, which we expect to produce good results provided that: (1) the combination of (relaxed) constraints eliminate the adverse effects of local minima incurred during the previous FWI cycle; (2) sharp reflectors are introduced that are of the correct sign; (3) progress is made during the previous FWI cycle; and (4) the “fine scales” of the previous FWI cycle contribute to the “coarse scales” of the next cycle.

We also applied this approach to a portion of the SEAM model (Fehler and Keliher, 2011) that contains a single salt

body with a rugose top, steep sides, and a complicated base, and that contains considerable presalt structure. Figure 4b shows the true model. Synthetic acoustic data were generated from this model using 96 near-surface marine sources recorded on a single fixed spread of 8000 m length containing 196 receivers. The two-dimensional model measures 3000×8000 m, and the bandwidth of the acquisition and the inversion runs from 3 to 12 Hz. With this small model and small data set, the full inversion runs in a few hours on a single workstation.

Figure 4a shows the starting model. In this model, the water velocity and bathymetry are correct; the subsurface velocity model is one-dimensional and follows approximately the compaction trend of the background basin. The salt body is not present in the starting model, the seabed velocity is not correct, and the velocity model was not obtained by smoothing the true model. Parts of the synthetic data are badly cycle skipped in this model at the

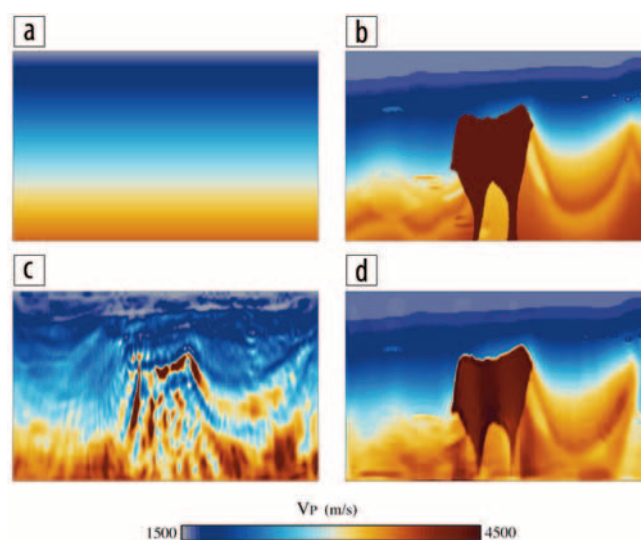


Figure 2. (a) Starting model; (b) true model; (c) FWI final model; (d) FWI + TV and asymmetric TV constraints final model.

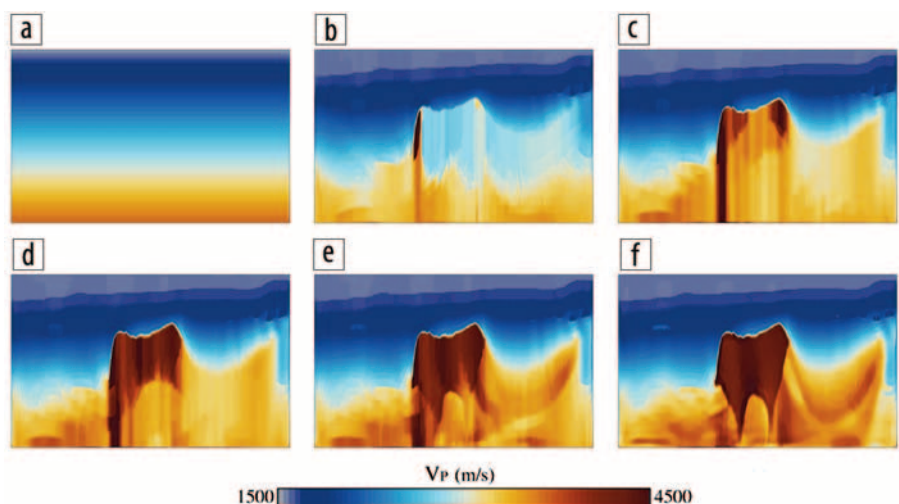


Figure 3. Snapshots for (a) the starting, and (b–f) the recovered velocity models, with one-sided TV continuation where the value of ξ/ξ_{true} is equal to (b) 0.01, (c) 0.1, (d) 0.2, (e) 0.5, and (f) 0.9. Adapted from Esser et al. (2015).

lowest frequencies available in the data, and conventional unconstrained FWI will fail inelegantly.

Figure 4c shows one result of applying conventional FWI to this data set. This has captured some of the characteristics of the true model, but this result is far from that true model. The recovered model represents a local minimum in the objective function, produced by a combination of cycle skipping and of more subtle effects related to the relative lack of turning energy and the difficulties of building sharply defined salt bodies within

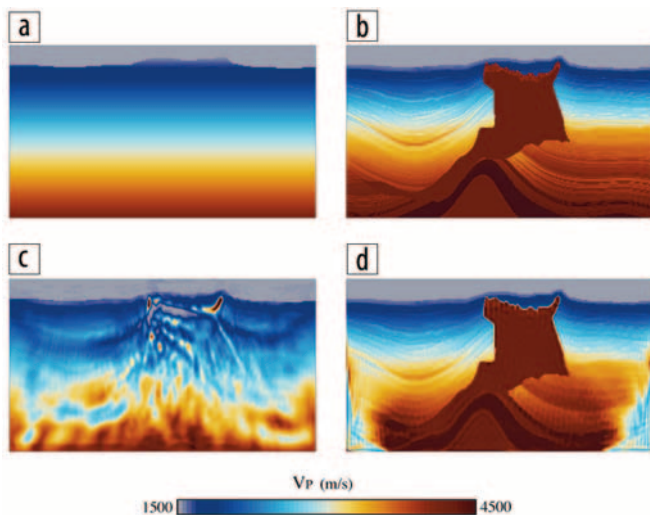


Figure 4. (a) Starting model; (b) portion of the Phase I SEAM model (Fehler and Keliher, 2011); (c) conventional unconstrained FWI result; and (d) TV and asymmetric TV-constrained FWI result.

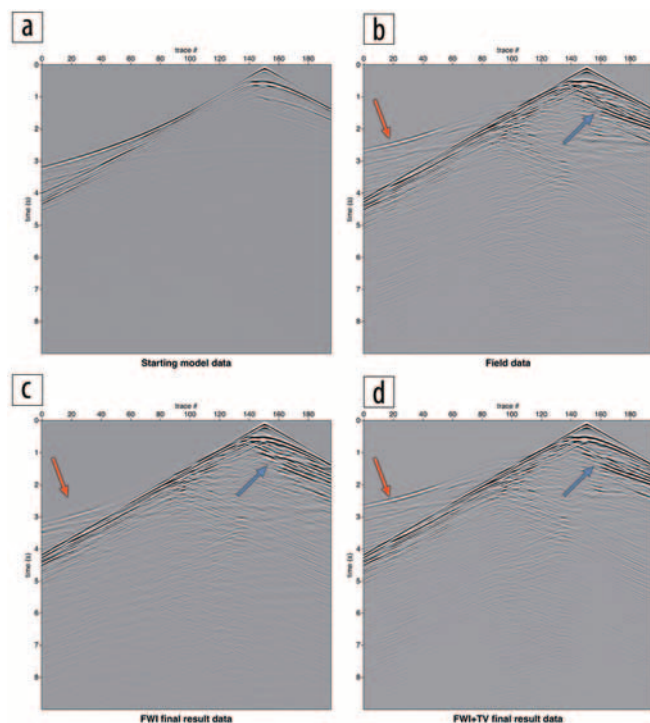


Figure 5. Shot records for (a) the starting model, (b) the true model, (c) final conventional unconstrained FWI result, and (d) the final hinge-loss constrained FWI result. Red and blue arrows highlight the parts of the data that are not properly matched with FWI without hinge-loss constraints.

otherwise smooth background models. The exact model generated by conventional FWI will vary in detail in response to the fine details of the FWI implementation, but any conventional FWI code will fail catastrophically for this combination of data and starting model.

Figures 5a, 5b, and 5c show a single shot record from the starting model, the final conventional FWI model, and the true model. While the data from the starting and true models are very different, many facets of the data from the final and true model are extremely similar. Especially at shorter offsets, this entirely erroneous velocity model is able to explain accurately much of the reflected and back-scattered energy; this figure illustrates one of the reasons that reflection traveltime tomography can have great difficulty in recovering useful velocity models from salt-affected data sets. The main features that are incorrectly matched by the erroneous model are the early fast-turning arrivals and some low-frequency short-offset arrivals seen most clearly at about 1700 m at about trace 150. These features are absent or badly cycle skipped in the recovered-model data.

Figure 6d shows the final model recovered by constrained FWI, using asymmetric hinge-loss applied in the vertical direction, conventional total variation applied in all directions, and fixed velocity bounds. These constraints have been relaxed progressively as the inversion proceeded through several warm restarts; for the final model these constraints play only a minor role. Their purpose is to guide the models generated in the early iterations toward geologically realistic outcomes, but, once that is achieved, it is the data that increasingly drives the final outcome. Figure 6 and the accompanying video show the evolution of the model as the inversion proceeds and the constraints are relaxed. Figure 5d shows a shot record produced from the final constrained-FWI model.

Clearly, the model recovered by constrained FWI is much closer to the true model than could be achieved by conventional FWI alone. The data generated by this model match the true data closely, and the cycle-skipped early arrivals at longer offsets have been captured correctly and reproduced by the model, as have the shorter-offset low-frequency arrivals. The inversion is able to capture the rugose top-salt boundary and the relatively uniform interior of the salt body; the constraints make no assumption about the velocity of the salt, and the FWI has recovered this velocity directly from the data.

More significantly, the model has captured the correct depth and geometry of bottom salt, the correct geometry of the salt flanks, and the correct long-wavelength velocity structure within the subsalt section. The velocity model contains some noise, but this is straightforward to remove using standard tools, and the recovered velocity model provides a good basis for subsequent accurate depth migration.

The evolution of the model, shown in Figure 6 and in the accompanying video, is interesting. At the very earliest iterations, the constraints are too strong, and they have the effect of largely wiping out the starting model while beginning to introduce a salt-like body that initially extends to the bottom of the model. As the constraints are relaxed, the salt body geometry develops, and the velocity within the salt moves toward that required by the data. The constraints initially mitigate against the formation of a bottom-salt boundary, but

once top salt and the salt interior are formed correctly, the data can overcome the weakening constraints and the bottom-salt and subsalt structure appears.

There are two important parameters that need to be chosen to make this scheme work effectively: the strength of the initial constraints and the rapidity with which those constraints are relaxed. A safe strategy is to start with strong constraints — which we do in this example — and to relax these constraints slowly. This strategy is always likely to work, but a more aggressive approach has the potential to converge to the same final answer in fewer total iterations. We are still exploring this trade-off.

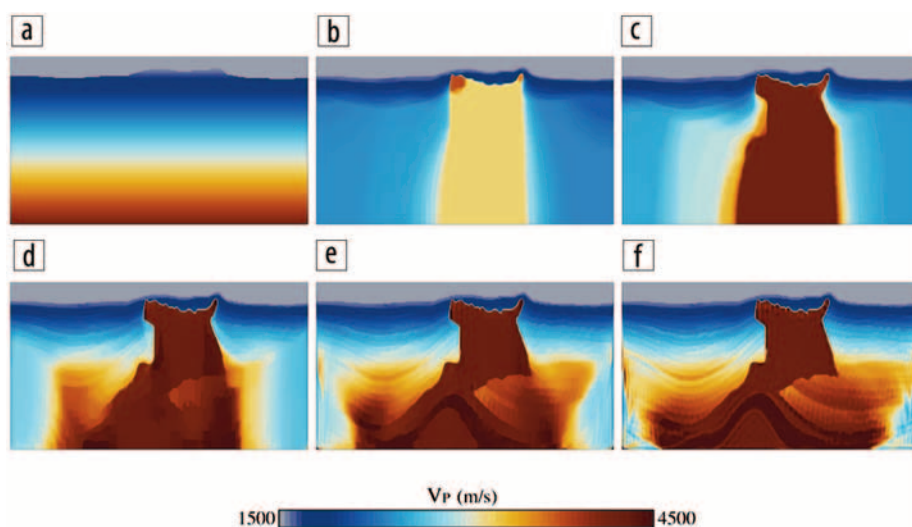


Figure 6. Evolution of the SEAM model from the starting point to the final recovered model as the constraints are relaxed. An accompanying video (viewable at <http://library.seg.org/doi/suppl/10.1190/tle35030235.1>) shows the full sequence of models.

Discussion and conclusions

We have shown that a suitably robust FWI code, when coupled with constrains based on both total variation and vertical hinge-loss asymmetric total-variation, can recover complex salt and subsalt velocity models starting from a simple one-dimensional velocity model without any manual intervention or picking. We hypothesize that the success of our method may well be explained by its conceptual similarity to existing manual workflows. At the start, the combination of our total-variation, hinge-loss norms and frequency-continuation acts to delineate top salt, Figure 3b. Next, subsequent iterations effectively carry out a salt flood that allows for a buildup of salt down to the bottom of the model, Figure 3c to 3d. As we continue to relax the hinge-loss constraint, negative-sign velocity updates increasingly are allowed to enter into the solution, which leads to a gradual buildup of velocity-lows under the salt, Figures 3e to 3f. The warm-started cycles in this automatic process correspond to the much more labor-intensive picking of bottom-salt reflections followed by tomographical velocity updates.

The examples we have shown here are synthetic, isotropic, and acoustic and therefore do not capture all the complications that arise within field data. Nonetheless, our results demonstrate the clear potential for constrained FWI to replace conventional velocity-model-building workflows bringing benefits in turnaround, cost, repeatability, accuracy, and resolution. ■■

Acknowledgments

The authors thank Sub Salt Solutions Limited for permission to publish this work. The use of hinge-loss total variation during geophysical inversion is the subject of a UK pending patent number 1509337.0.

Corresponding author: fherrmann@eos.ubc.ca

John “Ernie” Esser (May 19, 1980 – March 8, 2015)

The work presented in this paper is a tribute to its main author, Ernie Esser, who passed away in tragic circumstances last year. He was a young and very promising scientist with whom the coauthors had the privilege to collaborate.



References

- Billette, F. J., and S. Brandsberg-Dahl, 2005, The 2004 BP velocity benchmark: 67th EAGE Annual International Conference and Exhibition, Extended Abstracts.
- Esser, E., L. Guasch, T. van Leeuwen, A. Y. Aravkin, and F. J. Herrmann, 2015, Total variation regularization strategies in full waveform inversion for improving robustness to noise, limited data and poor initializations: Technical Report TR-EOAS-2015-5, 06 2015. <https://www.slim.eos.ubc.ca/Publications/Public/TechReport/2015/esser2015tvwri/esser2015tvwri.html>, accessed 16 February 2016.
- Fehler, M., and P. J. Keliher, 2011, Model Development, Chapter 2, 15–50, <http://dx.doi.org/10.1190/1.9781560802945.ch2>.
- Guo, Z., and M. V. de Hoop, 2013, Shape optimization and level set method in full waveform inversion with 3d body reconstruction: 83rd Annual International Meeting, SEG, Expanded Abstracts, 1079–1083, <http://dx.doi.org/10.1190/segam2013-1057.1>.
- Rudin, L. I., S. Osher, and E. Fatemi, 1992, Nonlinear total variation based noise removal algorithms: *Physica D. Nonlinear Phenomena*, **60**, no. 1–4, 259–268, [http://dx.doi.org/10.1016/0167-2789\(92\)90242-F](http://dx.doi.org/10.1016/0167-2789(92)90242-F).